

1 **Impact of in-cloud aqueous processes on the chemical**
2 **compositions and morphology of individual atmospheric**
3 **aerosols**

4 Yuzhen Fu^{1, 2}, Qin hao Lin^{1, #}, Guohua Zhang^{1, 3, *}, Yuxiang Yang^{1, 2}, Yiping Yang^{2, 4},
5 Xiufeng Lian^{1, 2}, Long Peng^{1, 2}, Feng Jiang^{1, 2, ##}, Xinhui Bi^{1, 3, *}, Lei Li⁵, Yuanyuan
6 Wang⁶, Duohong Chen⁷, Jie Ou⁸, Xinming Wang^{1, 3}, Ping'an Peng^{1, 3}, Jianxi Zhu⁴,
7 Guoying Sheng¹

8 ¹ State Key Laboratory of Organic Geochemistry and Guangdong Key Laboratory of Environmental
9 Protection and Resources Utilization, Guangzhou Institute of Geochemistry, Chinese Academy of
10 Sciences, Guangzhou 510640, PR China

11 ² University of Chinese Academy of Sciences, Beijing 100049, PR China

12 ³ Guangdong-Hong Kong-Macao Joint Laboratory for Environmental Pollution and Control, Guangzhou
13 510640, PR China

14 ⁴ CAS Key Laboratory of Mineralogy and Metallogeny & Guangdong Provincial Key Laboratory of
15 Mineral Physics and Materials, Guangzhou Institute of Geochemistry, CAS, Guangzhou 510640, PR
16 China

17 ⁵ Institute of Mass Spectrometer and Atmosphere Environment, Jinan University, Guangzhou 510632,
18 PR China

19 ⁶ Department of Atmospheric Science, School of Earth Science, Zhejiang University, Hangzhou 310027,
20 PR China

21 ⁷ State Environmental Protection Key Laboratory of Regional Air Quality Monitoring, Guangdong
22 Environmental Monitoring Center, Guangzhou 510308, PR China

23 ⁸ Shaoguan Environmental Monitoring Center, Shaoguan 512026, PR China

24 # now at: Guangdong Key Laboratory of Environmental Catalysis and Health Risk Control, Guangzhou
25 Key Laboratory Environmental Catalysis and Pollution Control, School of Environmental Science and
26 Engineering, Institute of Environmental Health and Pollution Control, Guangdong University of
27 Technology, Guangzhou 510006, PR China.

28 ## now at: Institute of Meteorology and Climate Research, Karlsruhe Institute of Technology, Eggenstein-
29 Leopoldshafen 76344, Germany.

30 *Correspondence to: Guohua Zhang (zhanggh@gig.ac.cn) and Xinhui Bi (bixh@gig.ac.cn)

31 **Abstract.** The composition, morphology, and mixing structure of individual cloud residues (RES) and interstitial
32 particles (INT) at a mountain-top site were investigated. Eight types of particles were identified, including sulfate-
33 rich (S-rich), S-organic matter (OM), aged soot, aged mineral, aged fly ash, aged metal, refractory, and aged
34 mixture. A shift of dominant particle types from S-rich (29%) and aged soot (27%) in the INT to S-OM (24%)
35 and aged mixture (22%) in the RES is observed. In particular, particles with organic shells are enriched in the
36 RES (30%) relative to the INT (12%). Our results highlight that the formation of more oxidized organic matter in
37 the cloud contributes to the existence of organic shells after cloud processing. We also show that in-cloud
38 processes may result in less compact soot, with the fractal dimensions (D_f) of soot in the RES (1.82 ± 0.12) lower
39 than those in the INT (2.11 ± 0.09). This research emphasizes the role of in-cloud processes on the chemistry and
40 microphysical properties of individual particles. Given that organic coatings may determine the particle
41 hygroscopicity, activation ability, and heterogeneous chemical reactivity, the increase of OM-shelled particles
42 upon in-cloud processes should have considerable implications.

43 1 Introduction

44 Aerosol-cloud interaction is regarded as one of the most significant sources of uncertainty in assessing the
45 radiative forcing of aerosols so far (IPCC, 2013). On the one hand, aerosols can participate in the formation of
46 cloud droplets, which is primarily influenced by their chemical composition and size at a certain supersaturation
47 (Fan et al., 2016; Maskey et al., 2017; Ogawa et al., 2016; Raymond and Pandis, 2002; Zelenyuk et al., 2010). On
48 the other hand, in-cloud processes, including the formation of sulfate, nitrate, and water-soluble organics, and the
49 physical processes such as collision and coagulation, would substantially change the physical and chemical
50 properties of the activated particles (Kim et al., 2019; Ma et al., 2013; Roth et al., 2016; Wu et al., 2013). Given
51 that the morphology and mixing state are vital in determining the optical properties of particles (Adachi et al.,
52 2010; Wu et al., 2018), changes of these properties upon in-cloud processes would further affect the subsequent
53 atmospheric processes (e.g., cloud activation, heterogeneous reactions) and radiative forcing of particles after
54 droplet evaporation.

55 Understanding the morphology and mixing state of particles upon in-cloud processes is of considerable
56 significance to improve the knowledge of aerosol-cloud interactions. For instance, Zelenyuk et al. (2010) found
57 that both cloud droplet residues (RES) and interstitial particles (INT, or unactivated particles in the cloud) are
58 mainly composed of organics, sulfate, biomass burning particles, and processed sea salt at the North Slope of
59 Alaska. Kamphus et al. (2010) observed that 92% of RES are particles containing sulfates, organics, and nitrate
60 at the Jungfrauoch (Swiss Alps). At Mt. Tai, Liu et al. (2018b) observed that main particle types are S (sulfate)-
61 soot (36%), S-fly ash/metal-soot (26%) and S-rich (24%) for RES and S-rich (61%), S-soot (15%) and soot (15%)
62 for INT. These results indicate that both RES and INT present complex mixtures, and carbonaceous matter (i.e.,
63 organic materials (OM) and soot) is important material in the cloud mass.

64 While there are extensive studies reporting the extent of aqueous phase processing on the modification of
65 aerosol bulk (e.g., mass) and/or chemical (e.g., mixing state, hygroscopicity) properties (Chakraborty et al., 2016;
66 Ervens et al., 2011), the influence of in-cloud processes on the physical properties (e.g., shape, mixing structure)
67 of individual particles is still ambiguous. In particular, physical properties can become dominant in the role of
68 cloud activation for particles with inorganic/organic mixed (Topping et al., 2007). A hydrophobic organic-rich
69 coating will form on a hygroscopic particle core if liquid-liquid phase separation occurs (Song et al., 2013).
70 Besides, the distribution of organics and its association with other aerosol types is also crucial for the correct
71 calculation of its radiative effects (Zhu et al., 2017). However, to what extent in-cloud processes play a role in
72 reshaping the distribution of organic and inorganic compositions remains unknown, although such coating
73 structures have been identified in ambient aerosols (Adachi and Buseck, 2008; Li and Shao, 2010; Yu et al., 2019).
74 Considering that in-cloud processes contribute to a substantial fraction (up to 60%) of organic aerosols (Ervens et
75 al., 2011; Liu et al., 2012; Myriokefalitakis et al., 2011; Spracklen et al., 2011), the influence of this process in
76 atmospheric chemistry cannot be neglected.

77 For another type of carbonaceous material, soot, there is extensive evidence that the absorption and cloud
78 activation of soot-containing particles can be significantly affected by coatings (Adachi et al., 2010; Wu et al.,

79 2018; Moffet and Prather, 2009). The critical factors to accurately predicting of such impact include the amount and
80 nature of the coating material, the exact particle morphology, and the size distribution (Qiu et al., 2012; Radney
81 et al., 2014). Fractal dimension (D_f) is widely used to indicate the extent of branching of soot (Brasil et al., 1999),
82 with densely packed or compacted soot particles having higher D_f than chain-like branched clusters or open
83 structures. While some studies have found that soot restructuring occurs after water processing (Bhandari et al.,
84 2019; Ma et al., 2013; Mikhailov et al., 2006), or being coated by OM (Spencer and Prather, 2006) and sulfate
85 (Zhang et al., 2008), Khalizov et al. (2013) suggested that soot with thin organic coating did not become more
86 compact under high humidity. However, the morphology and mixing structure of soot involving the formation of
87 organics upon cloud processing is also poorly constrained because of the limited field observation.

88 To further improve our understanding of the morphology and mixing structures between the various
89 components within individual RES and INT, we conducted a 25-day field observation of cloud events at a
90 background site in southern China. A transmission electron microscope (TEM) combined with energy-dispersive
91 X-ray spectrometry (EDS) was used to analyze the chemical composition, size, morphology, and mixing structure
92 of individual RES and INT. Previously, the chemical composition and mixing state of RES at the same site have
93 been investigated with a single particle aerosol mass spectrometer (SPAMS) (Lin et al., 2017; Zhang et al., 2017a).
94 Herein, we focus on the mixing structure (e.g., chemical compositions and morphology) of individual particles,
95 in particular, OM-containing particles. Meanwhile, particle types and mixing state of RES and INT are also
96 discussed. The difference between the mixing structure of RES and INT may indicate the impact of in-cloud
97 aqueous processes.

98 **2 Materials and Methods**

99 **2.1 Sampling site**

100 Sampling was conducted at the top of Mt. Tianjing (112°53'56" E, 24°41'56" N; 1690 m above sea level) in
101 southern China from 18 May to 11 June 2017. The sampling site is located in a natural preserve, and it is almost
102 unaffected by local anthropogenic sources. It is about 50 km and 350 km away from the north of the Pearl River
103 Delta (PRD) region and the South China Sea, respectively.

104 **2.2 Collection of RES and INT**

105 A cloud event was identified with visibility below a threshold of 3 km and relative humidity (RH) above a
106 threshold of 95%, using a ground-based counterflow virtual impactor (GCVI, model 1205, Brechtel Mfg. Inc.,
107 USA). The GCVI was automatically triggered when there was a cloud event, whereas it was not allowed to sample
108 when a precipitation sensor detected rain or snow. Then cloud droplets were introduced into the GCVI, followed
109 by removing water in an evaporation chamber (40 °C) to obtain RES. The sampling process might experience
110 some particle loss due to the evaporation of highly volatile substances. The droplet cut size, at which the
111 transmission efficiency of CVI was 50%, was set at a size larger than 7.5 μm (Shingler et al., 2012). INT was
112 sampled using another inlet (PM_{2.5} cyclone inlet, 5 lpm), followed by passing through a silica gel diffusion dryer.

113 A DKL-2 sampler (Genstar Electronic Technology Co., Ltd., China) was used to collect RES and INT on copper
114 grids coated with carbon film with an airflow of 1 L min⁻¹. The collection efficiency of the sampler is 50% at 80
115 nm, assuming the particle density is 2 g cm⁻³. To avoid particle overlapping, the sampling duration was set within
116 10 minutes. All samples were placed in a sealed plastic sample box and stored in a desiccator at room temperature
117 for subsequent analysis.

118 The information about cloud events and samples are summarized in Table 1. We focused on three cloud events
119 (#1, #2, and #3), with a duration of 14, 34, and 47 hours, respectively. RES and INT samples from these cloud
120 events were analyzed, with INT not available for the cloud event #1. To minimize the influence of rapid change
121 of cloud condition, all the samples were collected during the stable and mature periods (Visibility < 100 m).

122 **2.3 TEM analysis of RES and INT**

123 Chemical composition, size, and morphology of individual RES and INT were characterized by a TEM (FEI
124 Talos F200S) operated at 200 kV. TEM/EDS is a very effective tool to analyze the microscopic characteristics of
125 individual particles. The resolution of images between 1 μm and 100 nm can be magnified from 7,000 to 36,000
126 fold, which depended on the size of particles. The EDS is coupled with TEM to detect the intensity of elements
127 heavier than carbon ($Z \geq 6$). The produced X-rays signal in the EDS system is detected by a silicon (Si) drift
128 detector (SSD), and thus Si is not considered in the discussion. Cu is also not considered due to the interference
129 from the copper grids. In the TEM vacuum chamber, some volatile substances (e.g., ammonium nitrate (NH₄NO₃)
130 and volatile organic matter) would be lost. Moreover, volatile materials are often sensitive to strong electron
131 beams. Due to the analysis error of volatile materials, TEM/EDS studies typically focus on refractory
132 compositions. Using an image analysis software (ImageJ), the equivalent circle diameters (ECD) of all particles
133 can be obtained from the scanned images from the TEM. For particles with rim, only the nucleus is counted,
134 because the rims contain only a small amount of OM. Overall, 780 particles, including RES and INT, were
135 analyzed.

136 Base on various element spectra, RES and INT were mainly classified as sulfate-rich (S-rich), carbonaceous
137 material, mineral, metal, and fly ash (Twohy and Anderson, 2008; Li et al., 2016). Elemental compositions of S-
138 rich were dominated by S and O, and some of them were associated with minor N, K and Na. Low intensity of N
139 could be due to the evaporation of ammonia nitrate under the high energy electron beam (Smith et al., 2012). This
140 led to the bubbly appearance of S-rich. In this case, S-rich represented secondary inorganic particles. The
141 elemental compositions of carbonaceous materials were characteristics of abundant C and minor O. Carbonaceous
142 materials were divided into soot and OM according to different morphology. Soot were composed of tens to
143 hundreds of carbon spheres ranging from 21 to 108 nm in diameter (average diameter was 47.7 nm), which often
144 displayed botryoidal aggregates. OM did not have chain-like structure, which generally exhibited amorphous state
145 and spherical or irregular shapes. Mineral particles were consisted of Si, Al, Ca, O and minor Fe. Mineral were
146 mainly clay, feldspar, calcite and gypsum, usually showing irregular shapes. Metal particles were represented as
147 Fe, Zn, Ti, Mn, or Ni. Metal particles were characteristic of spherical, rectangular or irregular morphologies. They
148 were largely from natural dust and industrial combustion (Silva et al., 2000; Ye et al., 2018). The presence of
149 spherical metal particles indicated that they experienced melting at high temperature (Giere et al., 2003; Giere et

150 al., 2006). Fly ash particles mainly contained Si, Al and O. Fly ash particles tended to be spherical in morphology
151 and they were generally produced from the process of coal combustion (Chen et al., 2012; Henry and Knapp,
152 1980).

153 2.4 SPAMS analysis of RES and INT

154 A SPAMS (Hexin Analytical Instrument Co., Ltd., Guangzhou, China) was used to analyze chemical
155 composition and size distribution of individual particles in real-time. Particles entering SPAMS were first focused
156 into a beam of particles, and then their vacuum dynamic size (D_{va}) were measured by two continuous diode
157 Nd:YAG laser beams (532 nm). Next, the pulsed laser (266 nm) was precisely triggered to ionize target particle
158 according to the intrinsic velocity of each particle. Finally, we obtained the information of individual particles
159 including vacuum dynamic particle size and the positive and negative ion mass spectrometry. The relative peak
160 area of characteristic peaks of specific material in the mass spectra is generally applied to indicate its relative
161 abundance in the particle.

162 2.5 Calculating morphology parameters of soot

163 The fractal dimension of soot is characterized in the following statistical scaling law (Brasil et al., 1999; Köylü
164 et al., 1995):

$$165 \quad N = k_g \left(\frac{2R_g}{d_p} \right)^{D_f}$$

166 where N is the number of monomers within a certain soot aggregate, k_g is the fractal pre-factor, R_g is the radius of
167 gyration, d_p is the diameter of the monomer, and D_f is the mass fractal dimension. R_g can be obtained by using a
168 simple relationship between R_g and L_{max} , the maximum length of the soot aggregate (Brasil et al., 1999):

$$169 \quad L_{max}/2R_g = 1.50 \pm 0.05$$

170 And, the number of monomers, N , can be calculated by a power-law correlation of projected area of monomer
171 and aggregate:

$$172 \quad N = k_a \left(\frac{A_a}{A_p} \right)^\alpha$$

173 where k_a is a constant, A_a and A_p are the projected area of aggregate and monomer, respectively, and α is an
174 empirical projected area exponent. The value of k_a and α depends on the degree of monomer overlap (δ) in the
175 aggregate (Oh and Sorensen, 1997), and δ can be determined by:

$$176 \quad \delta = \frac{2a}{l}$$

177 where a is monomer radius, and l is the center distance of adjacent monomers. The value of parameters including
178 a , l , A_a , A_p , L_{max} , and d_p can be obtained by analyzing TEM images. Then D_f can be calculated by the above four
179 formulas.

180 **3 Results and Discussion**

181 **3.1 Particle type and mixing state of RES and INT**

182 According to mixing state, RES and INT were divided into following eight types (Figure 1): S-rich, S-OM,
183 refractory (soot/mineral/metal/fly ash), aged soot (S/OM-soot), aged mineral (S/OM-mineral), aged metal (S/OM-
184 metal), aged fly ash (S/OM-fly ash), and aged mixture (S/OM-soot/mineral/metal/fly ash). S-rich or OM, generally
185 considered to be aged since they are mainly secondarily produced in the atmosphere, are internally mixed with
186 refractory materials (soot/mineral/metal/fly ash) (Canagaratna et al., 2007; Huang et al., 2012; Jiang et al., 2019).
187 Such internally mixed S/OM-refractory particles are named as aged refractory particles herein. Aged particle types
188 containing two or more refractory components are named as “aged mixture”. It is worth noting that refractory are
189 refractory particles without S-rich and OM.

190 Figure 2 shows the number fraction of different particle types in the RES and INT during cloud events #2 and
191 #3. S-rich, S-OM, aged soot, and aged mixture particles are dominant particle types. The most abundant particles
192 in the RES are aged mixture (23%), followed by S-OM (22%), aged soot (20%), S-rich (16%), aged metal (9%),
193 aged fly ash (5%), aged mineral (4%), and refractory (1%). Differently, INT is predominated by S-rich (29%),
194 aged soot (27%), S-OM (15%), aged mixture (10%), and the lesser percentage of aged fly ash (8%), refractory
195 (5%), aged mineral (4%), and aged metal (2%) were also observed. Among three cloud events, the RES are
196 dominated by S-OM in cloud event #1 and #2 and aged mixture particles in cloud event #3 (Figure 3). It is also
197 shown that the RES and INT analyzed by TEM/EDS can represent their compositions throughout cloud events #2
198 and #3, since such compositions were relatively stable throughout these periods (Figure S3).

199 The different air masses are expected to affect the distribution of particle types. The distribution of several types
200 of particles in the RES were observed to be divergent in different cloud events, corresponding to different air
201 masses, as shown in Figure 3 and Figure 4. The number fraction of OM-containing particles was the highest (81%)
202 in cloud event #2, which might be partly attributed to the higher concentration of O_3 during cloud event #2 (Table
203 S1). And the samples of cloud event #2 sampled at noon. Higher solar radiation at the sampling time might also
204 promote heterogeneous photochemical oxidation reactions during the cloud process and increased the generation
205 of OM within cloud droplets (Xu et al., 2017). Aged metal particles accounted a similar percentage (7-12%) for
206 three cloud events. The proportion of aged mineral during cloud event #1 (14%) was nearly four times those in
207 the other two cloud events. Aged fly ash particles had the highest proportion (10%) in cloud event #3 compared
208 with the other two cloud events, which is most probably influenced by the different air masses (Figure 4). Aged
209 mineral particles of cloud event #1 may be influenced by the long-distance transportation of dust from Southeast
210 Asia (Salam et al., 2003). Clearly, aged fly ash particles of cloud event #3 are associated with the air masses from
211 the PRD region with a dense distribution of industrial facilities there (Cao et al., 2006).

212 3.2 The morphology and mixing structure of carbonaceous particles

213 OM-containing particles, including all of S-OM particles, part of aged refractory (S-OM/OM-refractory) and
214 aged mixture (S-OM/OM-soot/mineral/metal/fly ash) particles, accounted for 60% of RES and 33% of INT during
215 cloud events #2 and #3. According to the mixing structures between OM and other materials (Figure 5), OM-
216 containing particles are classified into the following five categories: thinly coated (Figure 5b), core-shell (Figure
217 5c), embedded (Figure 5d), attached (Figure 5e) and homogenous-like (Figure 5f) structures (Li et al., 2016). A
218 particle is classified as thinly coated structure when wrapped with a thin layer of OM. The thickness of the OM
219 layer of thinly coated particles ranges from 12 to 150 nm. Generally, the shapes of OM-containing particles with
220 thinly coated structure are elliptical or irregular. The difference between the core-shell structure and thinly coated
221 structure is the relative thickness of OM: Core-shell structure possessed thicker organics than thinly coated
222 structure. The thickness of the shell varies from 86 to 2110 nm, and the ratio of the projected area of the shell to
223 particle ranges from 0.20 to 0.97. Moreover, OM-containing particles with core-shell structure are round.
224 Embedded structure refers to the particle with OM embedded in other materials (e.g., sulfate). The attached
225 structure refers to the particle of OM attached to other materials. The homogenous-like structure represents
226 particles with evenly mixed and no identifiable boundary between organic and non-organic matter.

227 The first most abundant particles are thinly coated geometry, comprising 53% of RES and 59% of INT during
228 cloud event #2 and #3, respectively. The second are core-shell particles for RES and attached particles for INT.
229 The percentage of core-shell particles in the RES is almost 2.5 times that in the INT (27% vs. 12%). Embedded
230 and homogenous-like particles account for minor proportions (< 4%) for both RES and INT.

231 Soot-containing particles, including all of aged soot particles (S/OM-soot) and part of refractory
232 (soot/mineral/metal/fly ash) and aged mixture particles (S/OM-soot/mineral/metal/fly ash), account for 36% of
233 RES and 39% of INT during cloud event #2 and #3, respectively. The fraction is consistent with the range of those
234 (< 30% – ~60%) observed at the same site by SPAMS (Zhang et al., 2017a). Most of the soot are distributed
235 around the periphery of particles (Figure S4). Figure 6 shows the D_f of soot within RES and INT of cloud event
236 #2 and #3. The result shows that the D_f of soot is smaller in the RES (1.82 ± 0.12) than in the INT (2.11 ± 0.09),
237 which means that soot is more branched in the RES. It is noted that 62.5% of all soot-containing particles with
238 clear boundaries are included in the D_f calculation since thick coating around soot might make the boundary of
239 monomers not clear enough (Bhandari et al., 2019). The obtained D_f are close to those (1.83 – 2.16) reported at a
240 background site (Wang et al., 2017). The D_f of soot in the RES and INT likely represents partly coated soot (1.82
241 ± 0.05) (Yuan et al., 2019) and embedded soot (2.16 ± 0.05) (Wang et al., 2017), respectively. In addition to
242 emission sources and coating processes, high relative humidity (RH) during nighttime is a critical factor to
243 increase the compactness of soot (Yuan et al., 2019).

244 3.3 In-cloud formation of OM

245 It can be seen from Figure 2 that a shift of dominant particle types from S-rich (29%) and aged soot (27%) in
246 the INT to the aged mixture (23%) and S-OM (22%) in the RES. In particular, the fraction of OM-containing
247 particles increases from 33% in the INT to 60% in the RES. It is unlikely due to the favorable activation of S-OM
248 or aged mixture, since mixing with OM generally lower the hygroscopicity of inorganic-dominant particles (e.g.,

249 S-rich) (Brooks et al., 2004; Pierce et al., 2012). OM coating at the same site has been shown to inhibit the CCN
250 activation of soot-containing particles (Zhang et al., 2017a). Instead, it is most probably attributed to the in-cloud
251 formation of OM on the surface of some S-rich particles, shifting the dominant particle type from S-rich to S-OM
252 particles. It can be supported by the relatively larger median size of S-OM particles (0.76 μm) than S-rich particles
253 (0.56 μm) (Figure S5), since in-cloud formation of OM is expected to enlarge the original S-rich particles (Pierce
254 et al., 2012).

255 In addition, the fraction of OM-containing particles with core-shell mixing structure in the RES is almost 2.5
256 times that in the INT (Figure 5a). Such a mixing structure is similar to those observed in the Arctic, background,
257 or rural atmosphere (Hiranuma et al., 2013; Li et al., 2016; Yu et al., 2019), but is different from other findings in
258 polluted areas where OM is typically mixed with sulfate (Li et al., 2016). It is also consistent with several
259 laboratory simulations demonstrating that reactive uptake of volatile organic compounds (VOCs) on inorganic
260 sulfate and heterogeneous and multiphase reactions between these species would lead to a core-shell morphology
261 (e.g., Zhang et al., 2018; Riva et al., 2019; Zhang et al., 2019). Recently, Gorkowski et al. (2020) came up with a
262 particle morphology prediction framework developed for mixtures of organic aerosol based on the measurements
263 from aerosol optical tweezers experiments and literature data, and they hypothesized the core-shell morphology
264 dominated by secondary organic aerosols (SOA) in the shell phase.

265 Moreover, we estimated the O/C ratio of coating and shell within OM-containing particles. It should be noted
266 that the O/C ratio of organic coating and shell is underestimated herein due to the copper grid evenly covered by
267 carbon film. And, while some loss of volatile organic compounds during the TEM/EDS analysis may affect the
268 O/C of particles, the relatively higher O/C ratio for the RES is still affirmative. Droplets are expected to dissolve
269 more abundance of volatile organic compounds (Chakraborty et al., 2016), evaporation of which would result in
270 an underestimate of O/C to a higher degree rather than the INT. We found that the average value of the O/C ratio
271 of RES is higher than INT, and the average value of the O/C ratio of RES with core-shell structure is 0.23, which
272 is two times that with thinly coated structure (0.11) (Table 2), indicating that these RES with core-shell particles
273 are more oxidized. At the same site, we have previously observed enhanced aqueous SOA, such as oxalate in the
274 cloud (Zhang et al., 2017b). Higher O/C ratio of core-shell particles is also consistent with current studies reporting
275 more oxidized organic species in cloud/fog residues (Brege et al., 2018; Chakraborty et al., 2016; Zhang et al.,
276 2017b). With high levels of VOCs at the sampling site (Lv et al., 2019), prevalent formation of aqueous SOA
277 through the uptake of VOCs in cloud droplets would be expected (Kim et al., 2019; Liu et al., 2018a). The
278 contribution from photochemical processes may also be reflected by the association of the highest fraction (81%)
279 of OM-containing particles with a higher concentration of O_3 during cloud event #2 (Table S1).

280 However, one may expect that such core-shell mixing structure in the RES can also be explained by the primary
281 activation of S-OM particles with larger sizes. Unfortunately, no sample is available before cloud events. However,
282 with evidence from the collocated SPAMS, we show that this is not convincing. As shown in Table S2, the ratios
283 of relative peak area between organics and sulfate are similar between the INT and particles before cloud event,
284 whereas they are higher in the RES. This is corresponding to the production of oxidized organics during in-cloud
285 processes (Zhang et al., 2017b).

286 3.4 The D_f of soot in the RES and INT

287 While some previous studies demonstrated that soot aggregates tend to be more compact (with larger D_f) after
288 aging or cloud processing (Adachi and Buseck, 2013; Wu et al., 2018; Moffet and Prather, 2009), our results
289 suggest that in-cloud processes may result in more branched soot, as shown in Figure 6. Considering that D_f is
290 controlled mainly by emission sources, combustion conditions, and aging processes (Adachi et al., 2007), we
291 propose three possible explanations for the lower D_f of soot in the RES than that in the INT. The first and the most
292 likely reason is that some of the soot aggregates are immediately encapsulated by non-volatile materials (such as
293 organic matter) after emission by combustion sources. These coatings fill the spaces between the branches of soot
294 aggregates, which inhibits the relatively large deformation and reconfiguration of the soot aggregates during
295 transport and activation into cloud droplets (Zhang et al., 2018). Differently, soot aggregates may shrink easily
296 and become more compact during long-distance transport, if the soot aggregates are emitted without non-volatile
297 coatings (Adachi and Buseck, 2013). We show that soot aggregates have higher D_f and lower average ECD in the
298 INT (247 nm) than in the RES (266 nm), which means that larger, less dense soot particles are easier to act as
299 CCN. This is consistent with a study reporting that small particles are more compact than large particles (Adachi
300 et al., 2014). The second is that water-soluble substances within aerosols will be miscible after activating to cloud
301 droplets (Gorkowski et al., 2020), and the coating materials of soot may be released, which makes soot more
302 branched in the droplets and the following-up droplet evaporation. The third possible explanation is that different
303 combustion materials and combustion conditions produce soot-containing particles with different mixing states
304 and morphology (China et al., 2014; Khalizov et al., 2013; Liu et al., 2017; Zhang et al., 2018).

305 This result is in contrast to the current study reporting that soot sampled after cloud droplet evaporating are
306 more compact than freshly emitted and interstitial soot (Bhandari et al., 2019). Our observations at the background
307 site show that the majority of soot aggregates in both RES and INT (~80%) are located in off-center positions
308 (Figure S4), having less compact shapes even after being coated. This is quite different from the core-shell model
309 currently used in the climate models (Bond and Bergstrom, 2006; Wu et al., 2018). Through theoretical calculation,
310 Adachi et al. (2010) suggested that absorption cross-sections could be reduced by 20-30% with off-center
311 positions of soot relative to center positions. This means that the models based on core-shell assumption may
312 overestimate the absorption of soot-containing particles after cloud processing.

313 **4 Conclusion and atmospheric implications**

314 The result highlights the different morphology and mixing structures of activated and interstitial particles,
315 which may imply the substantial role of in-cloud aqueous processes in reshaping the activated particles. While Yu
316 et al. (2019) considered organic coatings on sulfate in the Arctic as a result of the increase of SOA following
317 particle aging and growth during transport, our data further imply a specific role of in-cloud processes in the
318 coating on sulfate. The prevalence of OM shelled particles after cloud processing also supports a current laboratory
319 observation depicting that rapid film formation and fast heterogeneous oxidation can provide an efficient way of
320 converting water-insoluble organic films into more water-soluble components in aerosols or cloud droplets
321 (Aumann and Tabazadeh, 2008).

322 Gorkowski et al. (2020) suggested that mixing structures of OM-containing particles are related to the oxidation
323 degree of OM. We also show that OM shells formed in-cloud have a higher degree of oxidation. Such a chemical

324 and morphological modification of aerosol particles may influence species diffusivities from the interior to the
325 surface region of the shell and gas-particle partitioning between the shell and gas (Liu et al., 2016; Shiraiwa et al.,
326 2013). Such a reshaping may also have an influence on aerosol hygroscopicity. Extrapolating the linear
327 relationship between the O/C ratio and the hygroscopicity parameter (κ_{org}) indicates that $\kappa_{\text{org-shell}}$ is about 1.4 times
328 $\kappa_{\text{org-coating}}$ (Jimenez et al., 2009; Lambe et al., 2011). In addition, the formation of the organic film could result in
329 a change of surface tension and thus affect the critical supersaturation required for particle activation (Ovadnevaite
330 et al., 2017). For mineral particles, the heterogeneous ice nucleation potential may be suppressed when coated by
331 OM (Möhler et al., 2008). Given the critical contribution of in-cloud aqueous SOA, several mixing structures of
332 OM-containing aerosols upon in-cloud processes may have substantial implications in modeling the direct and
333 indirect radiative forcing of aerosols (Scott et al., 2014; Zhu et al., 2017).

334

335 *Data availability.* Data are available on request from Guohua Zhang (zhanggh@gig.ac.cn) and Xinhui Bi
336 (bixh@gig.ac.cn).

337 *Author contribution.* GHZ and XHB designed the research (with input from XMW and GYS). YZF, GHZ, and
338 XHB analyzed the data, and wrote the manuscript. YZF, XFL, YXY, FJ, and QHL conducted sampling work
339 under the guidance of GHZ, XHB and XMW. LL, DHC and JO had an active role in supporting the sampling
340 work. YZF performed the laboratory analysis of individual particles by TEM/EDS, with support from YPY and
341 JXZ. All authors contributed to the discussions of the results and refinement of the manuscript.

342 *Competing interests.* The authors declare that they have no conflict of interest.

343 *Acknowledgements.* This work was supported by the National Nature Science Foundation of China (No. 41775124
344 and 41877307), Natural Science Foundation of Guangdong Province (2019B151502022), and Guangdong
345 Foundation for Program of Science and Technology Research (Grant No. 2019B121205006 and
346 2017B030314057). The authors gratefully acknowledge the NOAA Air Resources Laboratory (ARL) for the
347 provision of the HYSPLIT transport and dispersion model (<http://ready.arl.noaa.gov>) used in this publication.

348 **References**

- 349 Adachi, K., Chung, S. H., Friedrich, H., and Buseck, P. R.: Fractal parameters of individual soot particles
350 determined using electron tomography: Implications for optical properties, *Journal of Geophysical Research-*
351 *Atmospheres*, 112, D14202, 10.1029/2006jd008296, 2007.
- 352 Adachi, K., and Buseck, P. R.: Internally mixed soot, sulfates, and organic matter in aerosol particles from Mexico
353 City, *Atmospheric Chemistry and Physics*, 8, 6469-6481, 10.5194/acp-8-6469-2008, 2008.
- 354 Adachi, K., Chung, S. H., and Buseck, P. R.: Shapes of soot aerosol particles and implications for their effects on
355 climate, *Journal of Geophysical Research-Atmospheres*, 115, D15206, 10.1029/2009jd012868, 2010.
- 356 Adachi, K., and Buseck, P. R.: Changes of ns-soot mixing states and shapes in an urban area during CalNex,
357 *Journal of Geophysical Research-Atmospheres*, 118, 3723-3730, 10.1002/jgrd.50321, 2013.

358 Adachi, K., Zaizen, Y., Kajino, M., and Igarashi, Y.: Mixing state of regionally transported soot particles and the
359 coating effect on their size and shape at a mountain site in Japan, *Journal of Geophysical Research-Atmospheres*,
360 119, 5386-5396, 10.1002/2013jd020880, 2014.

361 Aumann, E., and Tabazadeh, A.: Rate of organic film formation and oxidation on aqueous drops, *Journal of*
362 *Geophysical Research-Atmospheres*, 113, D23205, 10.1029/2007jd009738, 2008.

363 Bhandari, J., China, S., Chandrakar, K. K., Kinney, G., Cantrell, W., Shaw, R. A., Mazzoleni, L. R., Giroto, G.,
364 Sharma, N., Gorkowski, K., Gilardoni, S., Decesari, S., Facchini, M. C., Zanca, N., Pavese, G., Esposito, F.,
365 Dubey, M. K., Aiken, A. C., Chakrabarty, R. K., Moosmüller, H., Onasch, T. B., Zaveri, R. A., Scarnato, B.
366 V., Fialho, P., and Mazzoleni, C.: Extensive Soot Compaction by Cloud Processing from Laboratory and Field
367 Observations, *Scientific reports*, 9, 11824-11824, 10.1038/s41598-019-48143-y, 2019.

368 Bond, T. C., and Bergstrom, R. W.: Light absorption by carbonaceous particles: An investigative review, *Aerosol*
369 *Science and Technology*, 40, 27-67, 10.1080/02786820500421521, 2006.

370 Brasil, A. M., Farias, T. L., and Carvalho, M. G.: A recipe for image characterization of fractal-like aggregates,
371 *Journal of Aerosol Science*, 30, 1379-1389, 10.1016/s0021-8502(99)00026-9, 1999.

372 Brege, M., Paglione, M., Gilardoni, S., Decesari, S., Facchini, M. C., and Mazzoleni, L. R.: Molecular insights on
373 aging and aqueous-phase processing from ambient biomass burning emissions-influenced Po Valley fog and
374 aerosol, *Atmospheric Chemistry and Physics*, 18, 13197-13214, 10.5194/acp-18-13197-2018, 2018.

375 Brooks, S. D., DeMott, P. J., and Kreidenweis, S. M.: Water uptake by particles containing humic materials and
376 mixtures of humic materials with ammonium sulfate, *Atmospheric Environment*, 38, 1859-1868,
377 10.1016/j.atmosenv.2004.01.009, 2004.

378 Canagaratna, M. R., Jayne, J. T., Jimenez, J. L., Allan, J. D., Alfarra, M. R., Zhang, Q., Onasch, T. B., Drewnick,
379 F., Coe, H., Middlebrook, A., Delia, A., Williams, L. R., Trimborn, A. M., Northway, M. J., DeCarlo, P. F.,
380 Kolb, C. E., Davidovits, P., and Worsnop, D. R.: Chemical and microphysical characterization of ambient
381 aerosols with the aerodyne aerosol mass spectrometer, *Mass Spectrometry Reviews*, 26, 185-222,
382 10.1002/mas.20115, 2007.

383 Cao, G., Zhang, X., and Zheng, F.: Inventory of black carbon and organic carbon emissions from China,
384 *Atmospheric Environment*, 40, 6516-6527, 10.1016/j.atmosenv.2006.05.070, 2006.

385 Chakraborty, A., Ervens, B., Gupta, T., and Tripathi, S. N.: Characterization of organic residues of size-resolved
386 fog droplets and their atmospheric implications, *Journal of Geophysical Research-Atmospheres*, 121, 4317-
387 4332, 10.1002/2015jd024508, 2016.

388 Chen, H., Laskin, A., Baltusaitis, J., Gorski, C. A., Scherer, M. M., and Grassian, V. H.: Coal fly ash as a source
389 of iron in atmospheric dust, *Environmental Science & Technology*, 46, 2112-2120, 10.1021/es204102f, 2012.

390 China, S., Salvadori, N., and Mazzoleni, C.: Effect of Traffic and Driving Characteristics on Morphology of
391 Atmospheric Soot Particles at Freeway On-Ramps, *Environmental Science & Technology*, 48, 3128-3135,
392 10.1021/es405178n, 2014.

393 Ervens, B., Turpin, B. J., and Weber, R. J.: Secondary organic aerosol formation in cloud droplets and aqueous
394 particles (aqSOA): a review of laboratory, field and model studies, *Atmospheric Chemistry and Physics*, 11,
395 11069-11102, 10.5194/acp-11-11069-2011, 2011.

396 Fan, J., Wang, Y., Rosenfeld, D., and Liu, X.: Review of Aerosol-Cloud Interactions: Mechanisms, Significance,
397 and Challenges, *Journal of the Atmospheric Sciences*, 73, 4221-4252, 10.1175/jas-d-16-0037.1, 2016.

398 Giere, R., Carleton, L. E., and Lumpkin, G. R.: Micro- and nanochemistry of fly ash from a coal-fired power plant,
399 *American Mineralogist*, 88, 1853-1865, 10.2138/am-2003-11-1228, 2003.

400 Giere, R., Blackford, M., and Smith, K.: TEM study of PM_{2.5} emitted from coal and tire combustion in a thermal
401 power station, *Environmental Science & Technology*, 40, 6235-6240, 10.1021/es060423m, 2006.

402 Gorkowski, K., Donahue, N. M., and Sullivan, R. C.: Aerosol Optical Tweezers Constrain the Morphology
403 Evolution of Liquid-Liquid Phase-Separated Atmospheric Particles, *Chem*, 6, 204-220,
404 10.1016/j.chempr.2019.10.018, 2020.

405 Henry, W. M., and Knapp, K. T.: Compound forms of fossil-fuel fly-ash emissions, *Environmental Science &*
406 *Technology*, 14, 450-456, 10.1021/es60164a010, 1980.

407 Hiranuma, N., Brooks, S. D., Moffet, R. C., Glen, A., Laskin, A., Gilles, M. K., Liu, P., Macdonald, A. M., Strapp,
408 J. W., and McFarquhar, G. M.: Chemical characterization of individual particles and residuals of cloud droplets
409 and ice crystals collected on board research aircraft in the ISDAC 2008 study, *Journal of Geophysical Research-*
410 *Atmospheres*, 118, 6564-6579, 10.1002/jgrd.50484, 2013.

411 Huang, H., Ho, K. F., Lee, S. C., Tsang, P. K., Ho, S. S. H., Zou, C. W., Zou, S. C., Cao, J. J., and Xu, H. M.:
412 Characteristics of carbonaceous aerosol in PM_{2.5}: Pearl Delta River Region, China, *Atmospheric Research*,
413 104, 227-236, 10.1016/j.atmosres.2011.10.016, 2012.

414 Intergovernmental Panel on Climate Change (IPCC) (2013), *Climate Change 2013: the physical science basis*,
415 Cambridge University Press, Cambridge, United Kingdom and New York, NY, USA, 2013

416 Jiang, F., Liu, F., Lin, Q., Fu, Y., Yang, Y., Peng, L., Lian, X., Zhang, G., Bi, X., Wang, X., and Sheng, G.:
417 Characteristics and Formation Mechanisms of Sulfate and Nitrate in Size-segregated Atmospheric Particles
418 from Urban Guangzhou, China, *Aerosol and Air Quality Research*, 19, 1284-1293, 10.4209/aaqr.2018.07.0251,
419 2019.

420 Jimenez, J. L., Canagaratna, M. R., Donahue, N. M., Prevot, A. S. H., Zhang, Q., Kroll, J. H., DeCarlo, P. F.,
421 Allan, J. D., Coe, H., Ng, N. L., Aiken, A. C., Docherty, K. S., Ulbrich, I. M., Grieshop, A. P., Robinson, A.
422 L., Duplissy, J., Smith, J. D., Wilson, K. R., Lanz, V. A., Hueglin, C., Sun, Y. L., Tian, J., Laaksonen, A.,
423 Raatikainen, T., Rautiainen, J., Vaattovaara, P., Ehn, M., Kulmala, M., Tomlinson, J. M., Collins, D. R.,
424 Cubison, M. J., Dunlea, E. J., Huffman, J. A., Onasch, T. B., Alfarra, M. R., Williams, P. I., Bower, K., Kondo,
425 Y., Schneider, J., Drewnick, F., Borrmann, S., Weimer, S., Demerjian, K., Salcedo, D., Cottrell, L., Griffin, R.,
426 Takami, A., Miyoshi, T., Hatakeyama, S., Shimono, A., Sun, J. Y., Zhang, Y. M., Dzepina, K., Kimmel, J. R.,
427 Sueper, D., Jayne, J. T., Herndon, S. C., Trimborn, A. M., Williams, L. R., Wood, E. C., Middlebrook, A. M.,
428 Kolb, C. E., Baltensperger, U., and Worsnop, D. R.: Evolution of Organic Aerosols in the Atmosphere, *Science*,
429 326, 1525-1529, 10.1126/science.1180353, 2009.

430 Kamphus, M., Ettner-Mahl, M., Klimach, T., Drewnick, F., Keller, L., Cziczo, D. J., Mertes, S., Borrmann, S.,
431 and Curtius, J.: Chemical composition of ambient aerosol, ice residues and cloud droplet residues in mixed-
432 phase clouds: single particle analysis during the Cloud and Aerosol Characterization Experiment (CLACE 6),
433 *Atmospheric Chemistry and Physics*, 10, 8077-8095, 10.5194/acp-10-8077-2010, 2010.

434 Khalizov, A. F., Lin, Y., Qiu, C., Guo, S., Collins, D., and Zhang, R.: Role of OH-Initiated Oxidation of Isoprene
435 in Aging of Combustion Soot, *Environmental Science & Technology*, 47, 2254-2263, 10.1021/es3045339,
436 2013.

437 Kim, H., Collier, S., Ge, X., Xu, J., Sun, Y., Jiang, W., Wang, Y., Herckes, P., and Zhang, Q.: Chemical processing
438 of water-soluble species and formation of secondary organic aerosol in fogs, *Atmospheric Environment*, 200,
439 158-166, 10.1016/j.atmosenv.2018.11.062, 2019.

440 Köylü, Ü. Ö., Xing, Y. C., and Rosner, D. E.: Fractal morphology analysis of combustion-generated aggregates
441 using angular light scattering and electron microscope images, *Langmuir*, 11, 4848-4854, 10.1021/la00012a043,
442 1995.

443 Lambe, A. T., Onasch, T. B., Massoli, P., Croasdale, D. R., Wright, J. P., Ahern, A. T., Williams, L. R., Worsnop,
444 D. R., Brune, W. H., and Davidovits, P.: Laboratory studies of the chemical composition and cloud
445 condensation nuclei (CCN) activity of secondary organic aerosol (SOA) and oxidized primary organic aerosol
446 (OPOA), *Atmospheric Chemistry and Physics*, 11, 8913-8928, 10.5194/acp-11-8913-2011, 2011.

447 Li, W., and Shao, L.: Mixing and water-soluble characteristics of particulate organic compounds in individual
448 urban aerosol particles, *Journal of Geophysical Research-Atmospheres*, 115, D02301, 10.1029/2009jd012575,
449 2010.

450 Li, W., Sun, J., Xu, L., Shi, Z., Riemer, N., Sun, Y., Fu, P., Zhang, J., Lin, Y., Wang, X., Shao, L., Chen, J., Zhang,
451 X., Wang, Z., and Wang, W.: A conceptual framework for mixing structures in individual aerosol particles,
452 *Journal of Geophysical Research-Atmospheres*, 121, 13784-13798, 10.1002/2016jd025252, 2016.

453 Lin, Q., Zhang, G., Peng, L., Bi, X., Wang, X., Brechtel, F. J., Li, M., Chen, D., Peng, P. a., Sheng, G., and Zhou,
454 Z.: In situ chemical composition measurement of individual cloud residue particles at a mountain site, southern
455 China, *Atmospheric Chemistry and Physics*, 17, 8473-8488, 10.5194/acp-17-8473-2017, 2017.

456 Liu, F., Bi, X., Zhang, G., Lian, X., Fu, Y., Yang, Y., Lin, Q., Jiang, F., Wang, X., Peng, P., and Sheng, G.: Gas-
457 to-particle partitioning of atmospheric amines observed at a mountain site in southern China, *Atmospheric*
458 *Environment*, 195, 1-11, 10.1016/j.atmosenv.2018.09.038, 2018a.

459 Liu, J., Horowitz, L. W., Fan, S., Carlton, A. G., and Levy, H., II: Global in-cloud production of secondary organic
460 aerosols: Implementation of a detailed chemical mechanism in the GFDL atmospheric model AM3, *Journal of*
461 *Geophysical Research-Atmospheres*, 117, D15303, 10.1029/2012jd017838, 2012.

462 Liu, L., Kong, S., Zhang, Y., Wang, Y., Xu, L., Yan, Q., Lingaswamy, A. P., Shi, Z., Lv, S., Niu, H., Shao, L.,
463 Hu, M., Zhang, D., Chen, J., Zhang, X., and Li, W.: Morphology, composition, and mixing state of primary
464 particles from combustion sources - crop residue, wood, and solid waste, *Scientific Reports*, 7, 5047,
465 10.1038/s41598-017-05357-2, 2017.

466 Liu, L., Zhang, J., Xu, L., Yuan, Q., Huang, D., Chen, J., Shi, Z., Sun, Y., Fu, P., Wang, Z., Zhang, D., and Li,
467 W.: Cloud scavenging of anthropogenic refractory particles at a mountain site in North China, *Atmospheric*
468 *Chemistry and Physics*, 18, 14681-14693, 10.5194/acp-18-14681-2018, 2018b.

469 Liu, P., Li, Y. J., Wang, Y., Gilles, M. K., Zaveri, R. A., Bertram, A. K., and Martin, S. T.: Lability of secondary
470 organic particulate matter, *Proceedings of the National Academy of Sciences of the United States of America*,
471 113, 12643-12648, 10.1073/pnas.1603138113, 2016.

472 Lv, S., Gong, D., Ding, Y., Lin, Y., Wang, H., Ding, H., Wu, G., He, C., Zhou, L., Liu, S., Ristovski, Z., Chen,
473 D., Shao, M., Zhang, Y., and Wang, B.: Elevated levels of glyoxal and methylglyoxal at a remote mountain site
474 in southern China: Prompt in-situ formation combined with strong regional transport, *The Science of the total*
475 *environment*, 672, 869-882, 10.1016/j.scitotenv.2019.04.020, 2019.

476 Ma, X., Zangmeister, C. D., Gigault, J., Mulholland, G. W., and Zachariah, M. R.: Soot aggregate restructuring
477 during water processing, *Journal of Aerosol Science*, 66, 209-219, 10.1016/j.jaerosci.2013.08.001, 2013.

478 Maskey, S., Chong, K. Y., Seo, A., Park, M., Lee, K., and Park, K.: Cloud Condensation Nuclei Activation of
479 Internally Mixed Black Carbon Particles, *Aerosol and Air Quality Research*, 17, 867-877,
480 10.4209/aaqr.2016.06.0229, 2017.

481 Mikhailov, E. F., Vlasenko, S. S., Podgorny, I. A., Ramanathan, V., and Corrigan, C. E.: Optical properties of
482 soot-water drop agglomerates: An experimental study, *Journal of Geophysical Research-Atmospheres*, 111,
483 D07209, 10.1029/2005jd006389, 2006.

484 Moffet, R. C., and Prather, K. A.: In-situ measurements of the mixing state and optical properties of soot with
485 implications for radiative forcing estimates, *Proceedings of the National Academy of Sciences of the United*
486 *States of America*, 106, 11872-11877, 10.1073/pnas.0900040106, 2009.

487 Möhler, O., Benz, S., Saathoff, H., Schnaiter, M., Wagner, R., Schneider, J., Walter, S., Ebert, V., and Wagner,
488 S.: The effect of organic coating on the heterogeneous ice nucleation efficiency of mineral dust aerosols,
489 *Environmental Research Letters*, 3, 025007, 10.1088/1748-9326/3/2/025007, 2008.

490 Myriokefalitakis, S., Tsigaridis, K., Mihalopoulos, N., Sciare, J., Nenes, A., Kawamura, K., Segers, A., and
491 Kanakidou, M.: In-cloud oxalate formation in the global troposphere: a 3-D modeling study, *Atmospheric*
492 *Chemistry and Physics*, 11, 5761-5782, 10.5194/acp-11-5761-2011, 2011.

493 Ogawa, S., Setoguchi, Y., Kawana, K., Nakayama, T., Ikeda, Y., Sawada, Y., Matsumi, Y., and Mochida, M.:
494 Hygroscopicity of aerosol particles and CCN activity of nearly hydrophobic particles in the urban atmosphere
495 over Japan during summer, *Journal of Geophysical Research-Atmospheres*, 121, 7215-7234,
496 10.1002/2015jd024636, 2016.

497 Oh, C., and Sorensen, C. M.: The effect of overlap between monomers on the determination of fractal cluster
498 morphology, *Journal of Colloid and Interface Science*, 193, 17-25, 10.1006/jcis.1997.5046, 1997.

499 Ovadnevaite, J., Zuend, A., Laaksonen, A., Sanchez, K. J., Roberts, G., Ceburnis, D., Decesari, S., Rinaldi, M.,
500 Hodas, N., Facchini, M. C., Seinfeld, J. H., and Dowd, C. O.: Surface tension prevails over solute effect in
501 organic-influenced cloud droplet activation, *Nature*, 546, 637-641, 10.1038/nature22806, 2017.

502 Pierce, J. R., Leaitch, W. R., Liggio, J., Westervelt, D. M., Wainwright, C. D., Abbatt, J. P. D., Ahlm, L., Al-
503 Basheer, W., Cziczo, D. J., Hayden, K. L., Lee, A. K. Y., Li, S. M., Russell, L. M., Sjostedt, S. J., Strawbridge,
504 K. B., Travis, M., Vlasenko, A., Wentzell, J. J. B., Wiebe, H. A., Wong, J. P. S., and Macdonald, A. M.:
505 Nucleation and condensational growth to CCN sizes during a sustained pristine biogenic SOA event in a
506 forested mountain valley, *Atmospheric Chemistry and Physics*, 12, 3147-3163, 10.5194/acp-12-3147-2012,
507 2012.

508 Qiu, C., Khalizov, A. F., and Zhang, R.: Soot Aging from OH-Initiated Oxidation of Toluene, *Environmental*
509 *Science & Technology*, 46, 9464-9472, 10.1021/es301883y, 2012.

510 Radney, J. G., You, R., Ma, X., Conny, J. M., Zachariah, M. R., Hodges, J. T., and Zangmeister, C. D.:
511 Dependence of Soot Optical Properties on Particle Morphology: Measurements and Model Comparisons,
512 *Environmental Science & Technology*, 48, 3169-3176, 10.1021/es4041804, 2014.

513 Raymond, T. M., and Pandis, S. N.: Cloud activation of single-component organic aerosol particles, *Journal of*
514 *Geophysical Research-Atmospheres*, 107, D24, 10.1029/2002jd002159, 2002.

515 Riva, M., Chen, Y., Zhang, Y., Lei, Z., Olson, N. E., Boyer, H. C., Narayan, S., Yee, L. D., Green, H. S., Cui, T.,
516 Zhang, Z., Baumann, K., Fort, M., Edgerton, E., Budisulistiorini, S. H., Rose, C. A., Ribeiro, I. O., e Oliveira,
517 R. L., dos Santos, E. O., Machado, C. M. D., Szopa, S., Zhao, Y., Alves, E. G., de Sá, S. S., Hu, W., Knipping,
518 E. M., Shaw, S. L., Duvoisin Junior, S., de Souza, R. A. F., Palm, B. B., Jimenez, J.-L., Glasius, M., Goldstein,
519 A. H., Pye, H. O. T., Gold, A., Turpin, B. J., Vizuete, W., Martin, S. T., Thornton, J. A., Dutcher, C. S., Ault,
520 A. P., and Surratt, J. D.: Increasing Isoprene Epoxydiol-to-Inorganic Sulfate Aerosol Ratio Results in Extensive
521 Conversion of Inorganic Sulfate to Organosulfur Forms: Implications for Aerosol Physicochemical Properties,
522 *Environmental Science & Technology*, 53, 8682-8694, doi:10.1021/acs.est.9b01019, 2019.

523 Roth, A., Schneider, J., Klimach, T., Mertes, S., van Pinxteren, D., Herrmann, H., and Borrmann, S.: Aerosol
524 properties, source identification, and cloud processing in orographic clouds measured by single particle mass
525 spectrometry on a central European mountain site during HCCT-2010, *Atmospheric Chemistry and Physics*,
526 16, 505-524, 10.5194/acp-16-505-2016, 2016.

527 Salam, A., Bauer, H., Kassin, K., Ullah, S. M., and Puxbaum, H.: Aerosol chemical characteristics of a mega-city
528 in Southeast Asia (Dhaka-Bangladesh), *Atmospheric Environment*, 37, 2517-2528, 10.1016/s1352-
529 2310(03)00135-3, 2003.

530 Scott, C. E., Rap, A., Spracklen, D. V., Forster, P. M., Carslaw, K. S., Mann, G. W., Pringle, K. J., Kivekäs, N.,
531 Kulmala, M., Lihavainen, H., and Tunved, P.: The direct and indirect radiative effects of biogenic secondary
532 organic aerosol, *Atmospheric Chemistry and Physics*, 14, 447-470, 10.5194/acp-14-447-2014, 2014.

533 Shingler, T., Dey, S., Sorooshian, A., Brechtel, F. J., Wang, Z., Metcalf, A., Coggon, M., Mülmenstädt, J., Russell,
534 L. M., Jonsson, H. H., and Seinfeld, J. H.: Characterisation and airborne deployment of a new counterflow
535 virtual impactor inlet, *Atmospheric Measurement Techniques*, 5, 1259-1269, 10.5194/amt-5-1259-2012, 2012.

536 Shiraiwa, M., Zuend, A., Bertram, A. K., and Seinfeld, J. H.: Gas-particle partitioning of atmospheric aerosols:
537 interplay of physical state, non-ideal mixing and morphology, *Physical Chemistry Chemical Physics*, 15,
538 11441-11453, 10.1039/c3cp51595h, 2013.

539 Silva, P. J., Carlin, R. A., and Prather, K. A.: Single particle analysis of suspended soil dust from Southern
540 California, *Atmospheric Environment*, 34, 1811-1820, 10.1016/s1352-2310(99)00338-6, 2000.

541 Smith, S., Ward, M., Lin, R., Brydson, R., Dall'Osto, M., and Harrison, R. M.: Comparative study of single particle
542 characterisation by Transmission Electron Microscopy and time-of-flight aerosol mass spectrometry in the
543 London atmosphere, *Atmospheric Environment*, 62, 400-407, 10.1016/j.atmosenv.2012.08.028, 2012.

544 Song, M., Marcolli, C., Krieger, U. K., Lienhard, D. M., and Peter, T.: Morphologies of mixed
545 organic/inorganic/aqueous aerosol droplets, *Faraday Discussions*, 165, 289-316, 10.1039/c3fd00049d, 2013.

546 Spencer, M. T., and Prather, K. A.: Using ATOFMS to determine OC/EC mass fractions in particles, *Aerosol*
547 *Science and Technology*, 40, 585-594, 10.1080/02786820600729138, 2006.

548 Spracklen, D. V., Jimenez, J. L., Carslaw, K. S., Worsnop, D. R., Evans, M. J., Mann, G. W., Zhang, Q.,
549 Canagaratna, M. R., Allan, J., Coe, H., McFiggans, G., Rap, A., and Forster, P.: Aerosol mass spectrometer
550 constraint on the global secondary organic aerosol budget, *Atmospheric Chemistry and Physics*, 11, 12109-
551 12136, 10.5194/acp-11-12109-2011, 2011.

552 Topping, D. O., McFiggans, G. B., Kiss, G., Varga, Z., Facchini, M. C., Decesari, S., and Mircea, M.: Surface
553 tensions of multi-component mixed inorganic/organic aqueous systems of atmospheric significance:

554 measurements, model predictions and importance for cloud activation predictions, *Atmospheric Chemistry and*
555 *Physics*, 7, 2371-2398, 10.5194/acp-7-2371-2007, 2007.

556 Twohy, C. H., and Anderson, J. R.: Droplet nuclei in non-precipitating clouds: composition and size matter,
557 *Environmental Research Letters*, 3, 045002, 10.1088/1748-9326/3/4/045002, 2008.

558 Wang, Y., Liu, F., He, C., Bi, L., Cheng, T., Wang, Z., Zhang, H., Zhang, X., Shi, Z., and Li, W.: Fractal
559 Dimensions and Mixing Structures of Soot Particles during Atmospheric Processing, *Environmental Science*
560 *& Technology Letters*, 4, 487-493, 10.1021/acs.estlett.7b00418, 2017.

561 Wu, Y., Cheng, T., Liu, D., Allan, J. D., Zheng, L., and Chen, H.: Light Absorption Enhancement of Black Carbon
562 Aerosol Constrained by Particle Morphology, *Environmental Science & Technology*, 52, 6912-6919,
563 10.1021/acs.est.8b00636, 2018.

564 Wu, Z. J., Poulain, L., Henning, S., Dieckmann, K., Birmili, W., Merkel, M., van Pinxteren, D., Spindler, G.,
565 Mueller, K., Stratmann, F., Herrmann, H., and Wiedensohler, A.: Relating particle hygroscopicity and CCN
566 activity to chemical composition during the HCCT-2010 field campaign, *Atmospheric Chemistry and Physics*,
567 13, 7983-7996, 10.5194/acp-13-7983-2013, 2013.

568 Xu, W., Han, T., Du, W., Wang, Q., Chen, C., Zhao, J., Zhang, Y., Li, J., Fu, P., Wang, Z., Worsnop, D. R., and
569 Sun, Y.: Effects of aqueous-phase and photochemical processing on secondary organic aerosol formation and
570 evolution in Beijing, China, *Environmental Science & Technology*, 51, 762-770, 10.1021/acs.est.6b04498,
571 2017.

572 Ye, L., Huang, M., Zhong, B., Wang, X., Tu, Q., Sun, H., Wang, C., Wu, L., and Chang, M.: Wet and dry
573 deposition fluxes of heavy metals in Pearl River Delta Region (China): Characteristics, ecological risk
574 assessment, and source apportionment, *Journal of Environmental Sciences-China*, 70, 106-123,
575 10.1016/j.jes.2017.11.019, 2018.

576 Yu, H., Li, W., Zhang, Y., Tunved, P., Dall'Osto, M., Shen, X., Sun, J., Zhang, X., Zhang, J., and Shi, Z.: Organic
577 coating on sulfate and soot particles during late summer in the Svalbard Archipelago, *Atmospheric Chemistry*
578 *and Physics*, 19, 10433-10446, 10.5194/acp-19-10433-2019, 2019.

579 Yuan, Q., Xu, J., Wang, Y., Zhang, X., Pang, Y., Liu, L., Bi, L., Kang, S., and Li, W.: Mixing State and Fractal
580 Dimension of Soot Particles at a Remote Site in the Southeastern Tibetan Plateau, *Environmental Science &*
581 *Technology*, 53, 8227-8234, 10.1021/acs.est.9b01917, 2019.

582 Zelenyuk, A., Imre, D., Earle, M., Easter, R., Korolev, A., Leitch, R., Liu, P., Macdonald, A. M., Ovchinnikov,
583 M., and Strapp, W.: In Situ Characterization of Cloud Condensation Nuclei, Interstitial, and Background
584 Particles Using the Single Particle Mass Spectrometer, SPLAT II, *Analytical Chemistry*, 82, 7943-7951,
585 10.1021/ac1013892, 2010.

586 Zhang, G., Lin, Q., Peng, L., Bi, X., Chen, D., Li, M., Li, L., Brechtel, F. J., Chen, J., Yan, W., Wang, X., Peng,
587 P., Sheng, G., and Zhou, Z.: The single-particle mixing state and cloud scavenging of black carbon: a case study
588 at a high-altitude mountain site in southern China, *Atmospheric Chemistry and Physics*, 17, 14975-14985,
589 10.5194/acp-17-14975-2017, 2017a.

590 Zhang, G., Lin, Q., Peng, L., Yang, Y., Fu, Y., Bi, X., Li, M., Chen, D., Chen, J., Cai, Z., Wang, X., Peng, P.,
591 Sheng, G., and Zhou, Z.: Insight into the in-cloud formation of oxalate based on in situ measurement by single
592 particle mass spectrometry, *Atmospheric Chemistry and Physics*, 17, 13891-13901, 10.5194/acp-17-13891-
593 2017, 2017b.

594 Zhang, R., Khalizov, A. F., Pagels, J., Zhang, D., Xue, H., and McMurry, P. H.: Variability in morphology,
595 hygroscopicity, and optical properties of soot aerosols during atmospheric processing, *Proceedings of the*
596 *National Academy of Sciences of the United States of America*, 105, 10291-10296, 10.1073/pnas.0804860105,
597 2008.

598 Zhang, Y., Chen, Y., Lambe, A. T., Olson, N. E., Lei, Z., Craig, R. L., Zhang, Z., Gold, A., Onasch, T. B., Jayne,
599 J. T., Worsnop, D. R., Gaston, C. J., Thornton, J. A., Vizuete, W., Ault, A. P., and Surratt, J. D.: Effect of the
600 Aerosol-Phase State on Secondary Organic Aerosol Formation from the Reactive Uptake of Isoprene-Derived
601 Epoxydiols (IEPOX), *Environmental Science & Technology Letter*, 5, 167-174,
602 doi:10.1021/acs.estlett.8b00044, 2018.

603 Zhang, Y., Chen, Y., Lei, Z., Olson, N. E., Riva, M., Koss, A. R., Zhang, Z., Gold, A., Jayne, J. T., Worsnop, D.
604 R., Onasch, T. B., Kroll, J. H., Turpin, B. J., Ault, A. P., and Surratt, J. D.: Joint Impacts of Acidity and Viscosity
605 on the Formation of Secondary Organic Aerosol from Isoprene Epoxydiols (IEPOX) in Phase Separated
606 Particles, *ACS Earth Space Chem.*, 3, 2646-2658, doi:10.1021/acsearthspacechem.9b00209, 2019.

607 Zhang, Y., Yuan, Q., Huang, D., Kong, S., Zhang, J., Wang, X., Lu, C., Shi, Z., Zhang, X., Sun, Y., Wang, Z.,
608 Shao, L., Zhu, J., and Li, W.: Direct Observations of Fine Primary Particles From Residential Coal Burning:
609 Insights Into Their Morphology, Composition, and Hygroscopicity, *Journal of Geophysical Research-*
610 *Atmospheres*, 123, 12964-12979, 10.1029/2018jd028988, 2018.

611 Zhu, J., Penner, J. E., Lin, G., Zhou, C., Xu, L., and Zhuang, B.: Mechanism of SOA formation determines
612 magnitude of radiative effects, *Proceedings of the National Academy of Sciences of the United States of*
613 *America*, 114, 12685-12690, 10.1073/pnas.1712273114, 2017.

614 **Table 1. The information of cloud events and samples, including starting and ending time of each cloud event, the number and type of analyzed particles, the mean value**
 615 **of visibility and number concentration of RES or INT during sampling time.**
 616

Cloud event	Starting Time*	Ending Time*	Particles	Type	Visibility/m	Number Concentration/cm ⁻³
Cloud #1	2017/5/20 18:19	2017/5/21 8:34	190	RES	66	195
Cloud #2	2017/5/23 20:35	2017/5/25 6:35	161	INT	50	99
			162	RES	88	299
Cloud #3	2017/6/8 18:30	2017/6/10 17:30	132	INT	44	996
			135	RES	33	111

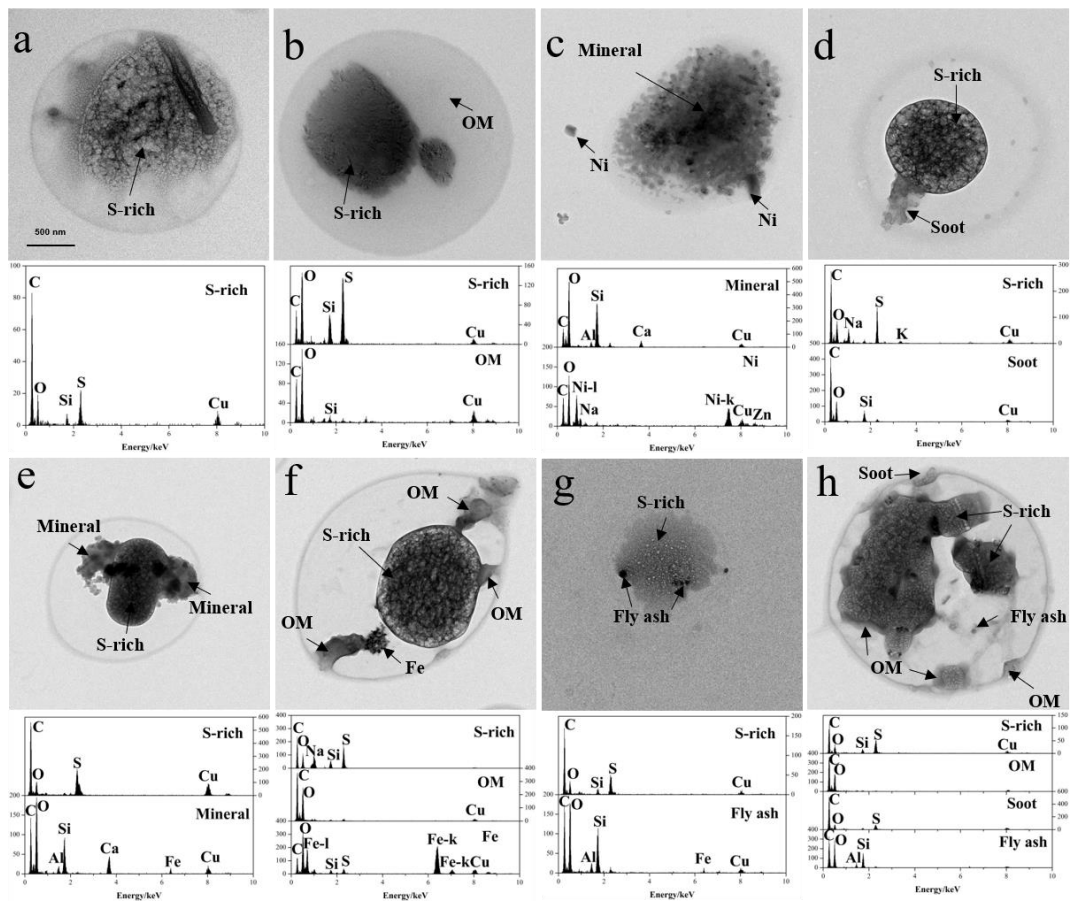
617 * The time is the local time and that is Chinese Standard Time, UTC+8.

618 **Table 2. The average value of O/C ratio of OM-containing particles with thinly coated and core-shell mixing structures.**

619

Type	thinly coated	core-shell
RES	0.11	0.23
INT	0.08	0.06

620

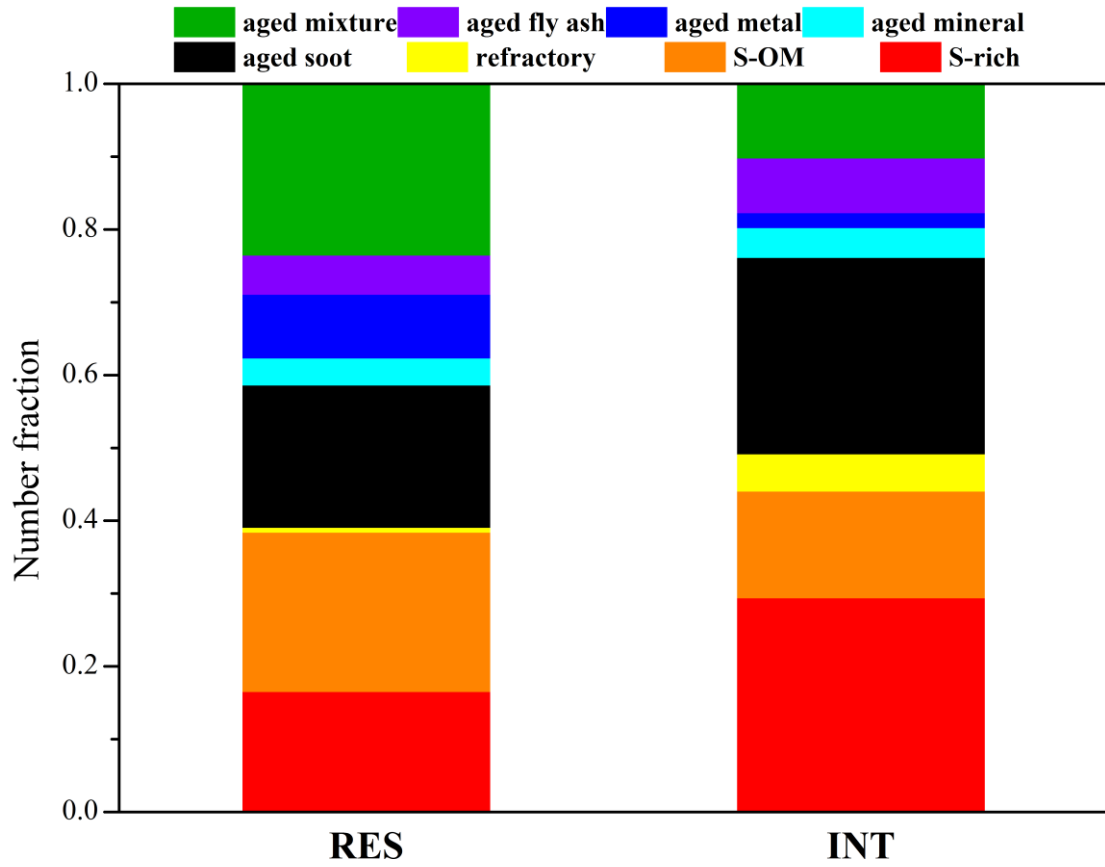


621

622 **Figure 1. TEM images and EDS spectra of individual RES and INT particles with different particle types: (a)**

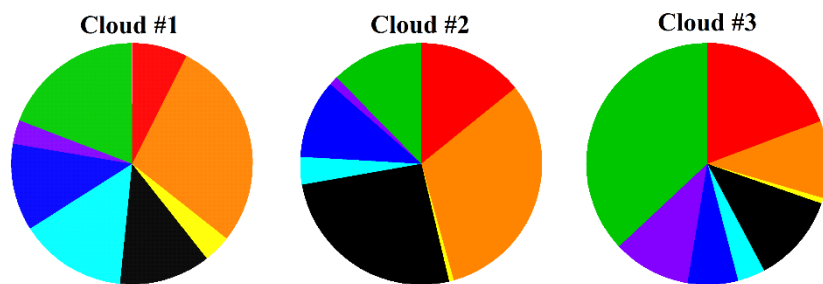
623 **S-rich; (b) S-OM; (c) refractory; (d) aged soot; (e) aged mineral; (f) aged metal; (g) aged fly ash; (h) aged**

624 **mixture.**



625

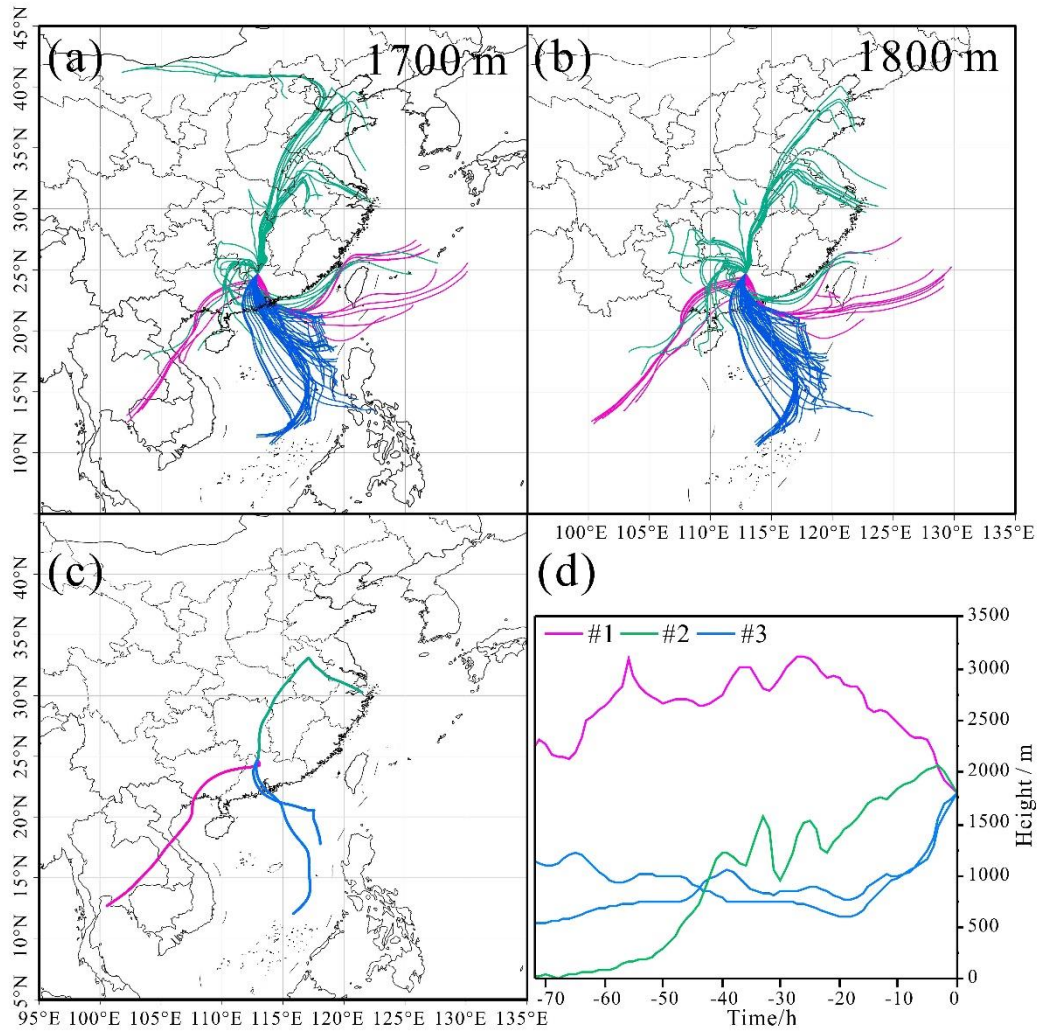
626 **Figure 2. Number fractions of different particle types in the RES and INT of cloud event #2 and #3 measured**
 627 **by TEM/EDS.**



628

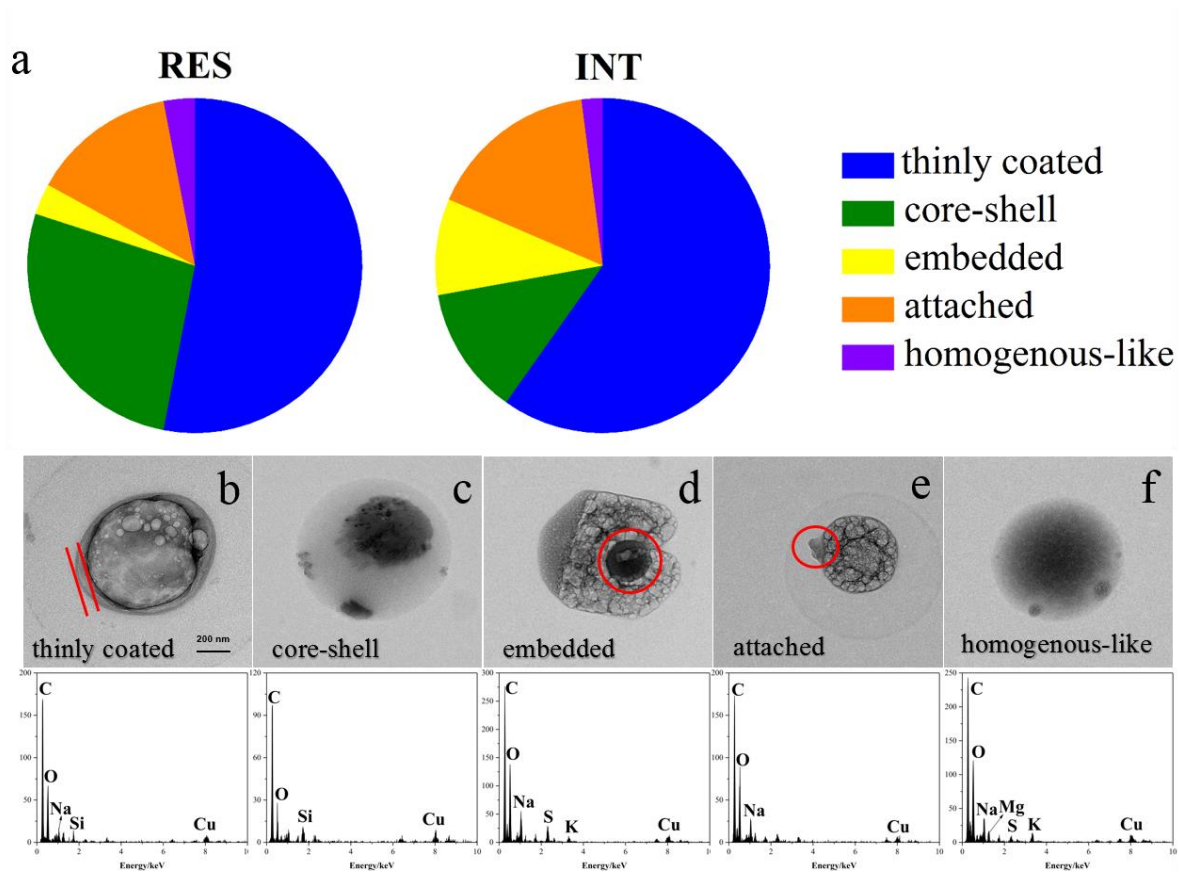
629 Figure 3. Number fraction of different particle types in the RES during three cloud events measured by

630 TEM/EDS.



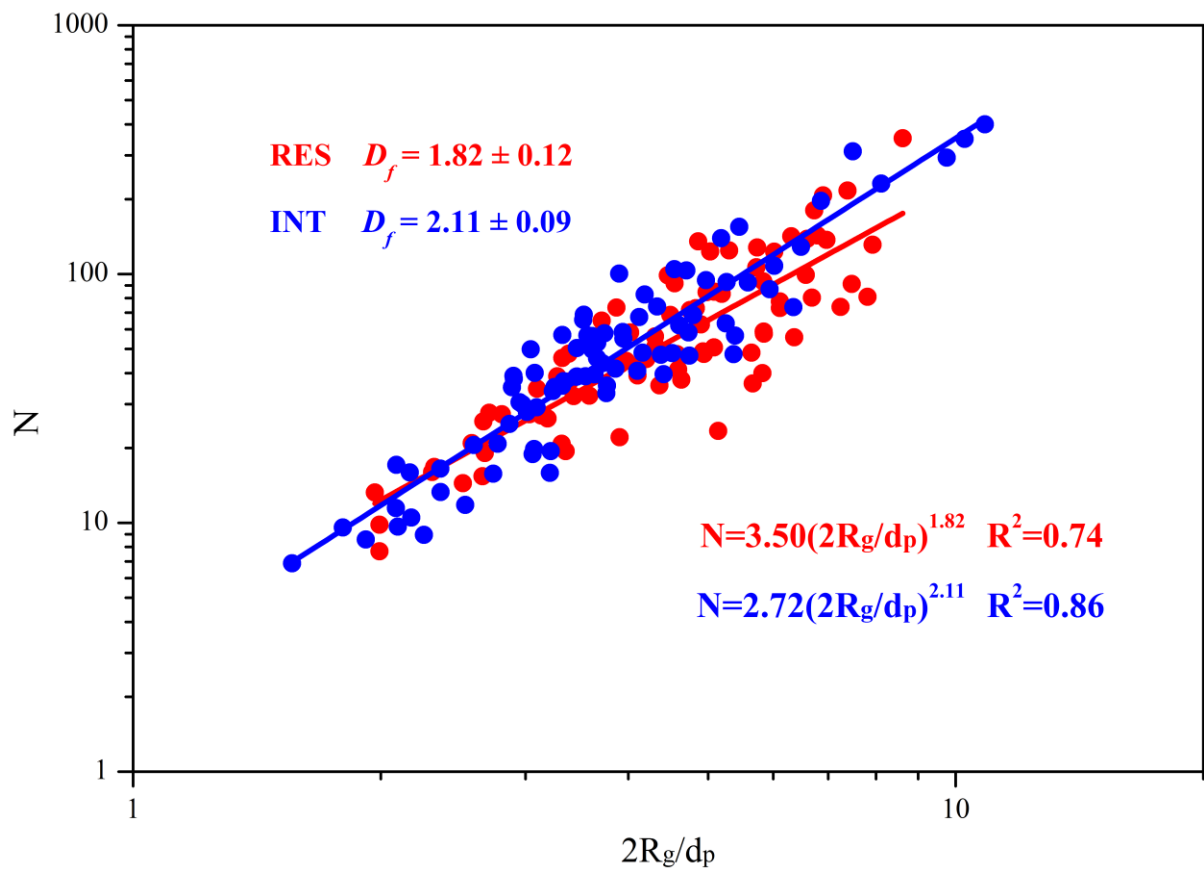
631

632 **Figure 4. HYSPLIT back trajectories (72 h) for air masses arriving at our sampling site at the height of 1700**
 633 **m (a) and 1800 m (b) hourly during the three cloud events. The HYSPLIT back trajectories at the height of**
 634 **1800 m during sampling periods (c) and heights (above sea level) of the air masses during transport (d). The**
 635 **horizontal axis represents several time points (0-72 h) before the time point input into the HYSPLIT model.**



636

637 Figure 5. Number fractions of OM-containing particles with different mixing structures in the RES and INT (a) and
 638 typical TEM images and corresponding EDS spectra of OM: thinly coated (b); core-shell (c); embedded
 639 (e); homogenous-like (f) during cloud event #2 and #3.



640

641

Figure 6. Fractal dimensions of soot in the RES and INT during cloud event #2 and #3.